International Journal of Solids and Structures 47 (2010) 2672–2679

Contents lists available at ScienceDirect

International Journal of Solids and Structures

journal homepage: www.elsevier.com/locate/ijsolstr

Dynamic response of tubular dielectric elastomer transducers

Seyul Son [a,b,*], N.C. Goulbourne [b]

[a] Center for Intelligent Material Systems and Structures, Virginia Polytechnic Institute and State University, Blacksburg, VA 24060, USA
[b] Soft Material Research Lab, Department of Aerospace Engineering, University of Michigan, Ann Arbor, MI 48109-2140, USA

ARTICLE INFO

Article history:
Received 4 January 2010
Received in revised form 18 May 2010
Available online 26 May 2010

Keywords:
Dielectric elastomer
Transducer
Membrane
Electroactive polymer and Maxwell stress

ABSTRACT

In this paper, a numerical model for the dynamic response of tubular dielectric elastomer transducers is presented and validated with experimental results for the first time. Dielectric elastomers (DE) are soft polymer based smart materials that can be potentially employed in applications such as actuation, sensing and energy harvesting (Kornbluh, 2004; Carpi et al., 2005; Waki et al., 2008). In our previous work, the quasi-static response of tubular DE transducers was studied (Goulbourne et al., 2007; Son and Goulbourne, 2009). Here, a numerical model is developed to predict the dynamic response of tubular DE transducers. Inertia effects are included in our previous static model which yields a system of partial differential equations. The results of the dynamic response of the tubular DE transducers are obtained by numerically solving the simplified partial different equations using a finite difference scheme. The capacitance change induced by the dynamic deformation of the tubular DE is also calculated by a simple electrostatic model, illustrating dynamic passive sensing.

Several tubular DE transducer samples (VHB 4905 and silicone) were fabricated and an experimental setup was developed to investigate the dynamic response by measuring capacitance and radial deformation. In the sensing experiments, a sweep of dynamic pressure profiles (0–5 Hz) are applied. It is observed that silicone transducers have a larger dynamic sensing range. In the actuation experiments, the deformation of the silicone actuator is monitored while a voltage signal (4.5 kV) is applied from 0 to 30 Hz. The silicone actuator shows a good actuation response. The comparison between numerical and experimental results for the DE transducers shows an overall error of 3%.

1. Introduction

The purpose of this research is to study the dynamic response of tubular dielectric elastomer transducers using both an experimental and numerical modeling approach. Dielectric elastomers can be employed as actuators, large strain sensors and for energy harvesting (Kornbluh, 2004; Carpi et al., 2005, 2008; Waki et al., 2008). Dielectric elastomer sensors are essentially compliant capacitors, which have a capacitance that varies with mechanical strain, or alternatively, the resistance can be monitored. In general, conventional sensor materials are relatively stiff and fail at low strains within 2.5–5.0%. Dielectric elastomer sensors provide various advantages such as large strain range, simple fabrication, low cost, low weight, repeatability and shape compliance (Pei et al., 2004; Rosenthal et al., 2007). Dielectric elastomer actuators are large strain electroactive polymers with areal strains up to 300% (Pelrine et al., 2000).

In the previous work, a finite deformation model for dielectric elastomer membranes in actuation mode was derived (Goulbourne et al., 2005). In this paper, a dynamic model for tubular configurations is derived by combining a modified large deformation membrane theory that accounts for the coupling electromechanical effect in actuation commonly referred to as the Maxwell stress and the dynamic capacitance change under finite strains which accounts for passive sensing is calculated. The equations are simplified with the assumption that the inertia effect in the meridional direction is negligible. The dynamic model consists of a set of PDEs (partial differential equations). A finite difference scheme (forward difference method) is used to simulate the dynamic response of the tubular DE transducer. The numerical method is general and can readily be employed for other axisymmetric configurations, and has a moderate computing time. The running time for the numerical method can be reduced by optimizing the finite difference algorithm.

Dynamic characterization of edge-clamped DE membrane actuators in a diaphragm configuration was conducted using an experimental approach in Fox (2007), Fox and Goulbourne (2008). The static response of tubular DE sensors was studied and numerical results were validated with experiments in Goulbourne et al. (2007), Goulbourne and Son (2008). Tubular DE transducers have

* Corresponding author at: Soft Material Research Lab, Department of Aerospace Engineering, University of Michigan, Ann Arbor, MI 48109-2140, USA. Tel.: +1 54 08089300.
E-mail address: sson@vt.edu (S. Son).

0020-7683/$ - see front matter © 2010 Elsevier Ltd. All rights reserved.
doi:10.1016/j.ijsolstr.2010.05.019

been previously analyzed by Carpi and De Rossi (2004), Pei et al. (2004). Carpi et al. proposed a static model for actuation which was validated within the small strain range (0–5.0%). The model was based on the linear elasticity theory (Carpi and De Rossi, 2004). An actuation characterization of spring roll DE actuators has been conducted using analysis techniques (Pei et al., 2004). The previous works have focused on the static actuation response and was limited to small strains. In this paper, a finite deformation model is used to describe the dynamic response of these transducers in both actuation and sensing modes (Adkins and Rivlin, 1955). For large elastic deformations, the developments by Adkins and Rivlin (1952, 1955), Kydoniefs (1968, 1969, 1972), Matsikoudi-Iliopoulou (1987) are most notable. The dynamic mechanical response of elastic membranes has been studied by Jenkins (1996), Tüzel and Erbay (2004), Verron et al. (1999), Verron et al. (2001) to name a few. Specifically, Jenkins et al. applied dynamic approaches to the dynamic inflation field while considering the membrane's inertia (Jenkins, 1996) and Tüzel studied the dynamic response of an isotropic hyperelastic membrane tube, subjected to a dynamic extension at one end (Tüzel and Erbay, 2004). Verron applied the Mooney–Rivlin model or nonlinear viscoelastic Christensen's model to the dynamic inflation of spherical membranes (Verron et al., 1999, 2001). The dynamic response of planar dielectric elastomer actuators was investigated in Sommer-Larsen et al. (2001) by measuring current change while a high voltage (~6 kV) was applied and the strain decrease of the DE actuator presumed due to material viscoelasticity was presented (Pei et al., 2003). Here the dynamic inflation of tubular membrane in the presence of an electric field are considered.

Experimental results are obtained to validate the proposed dynamic modeling approach. The experimental procedure is devised to measure the dynamic deformation and capacitance of the DE membrane in sensing mode, in actuation mode, and in simultaneous sensing and actuation mode. For dynamic sensing the electromechanical response is measured while a dynamic pressure was applied for various frequencies, 0–5.0 Hz. The tubular DE sensors are prepared with 3M VHB 4905 and silicone films (NuSil Technology: CF 19-2186), which are commercially available and spincoated in situ, respectively. They are electroded with carbon grease (Carbon Conductive Grease, M.G. Chemicals). Two end cylindrical shapes (Radius = 9.5 and Length = 10 mm) of the transducers are made of fluoropolymers (Teflon®PTFE, McMaster-Carr Supply Company). The dynamic pressure is generated for low frequencies (~2.5 Hz) and higher frequencies (2.5–5.0 Hz). A comparison between the dynamic behavior of the VHB and silicone sensors is presented. For the dynamic actuation behavior of tubular DEs, radial deformations of the tubular DE actuator are monitored while a dynamic voltage signal is applied with various frequencies, 0–30 Hz. In the actuation experiments, since VHB with radial prestretch did not show good actuation response while high voltage (4.5 kV) is applied, only silicone DEs are used in the actuation experiments.

2. Principle of dielectric elastomer transducer

Dielectric elastomers are large strain electromechanical transducers. The dielectric elastomer transducer is a three-component system consisting of a compliant elastomeric insulator sandwiched between two compliant electrodes. For the sensing configuration, mechanical strains are detected by measuring one of two electrical parameters: capacitance or resistance. These sensors are ideal for large strain sensing applications due to the ability to retain electrical conductivity at large strains – even up to 100%. For actuation, electrostatic forces are induced by applying an electric field to the dielectric elastomer. This results in thickness reduction and an areal expansion in the in-plane directions due to an effect that is amplified by the softness of the material and material incompressibility. A schematic of the typical assembly of a dielectric elastomer transducer as well as depiction of its sensing and actuation mode is given in Figs. 1a and 1b.

The two most common types of dielectric elastomers used in fabricating transducers are polyacrylates and silicone elastomers (Pelrine et al., 2000; Yang et al., 2005). Failure of a typical specimen of 3M VHB 4905 (polyacrylate) does not occur until a stretch ratio of 8. Applying compliant electrodes to the major surfaces of prestretched dielectric elastomer specimens completes the fabrication process. We have conducted an experimental evaluation of the large stretch response of different electrodes: carbon grease, silver grease, graphite powder, and graphite spray. The experimental results indicate that carbon grease and silver grease are the best compliant electrodes of the four that were tested; carbon grease has a slightly better overall performance and is also less costly (Fox and Goulbourne, 2006).

3. Electroelastic model

In this section, the modeling approach for the dynamic response of tubular DE transducer is presented. Specifically, the previous large deformation model for the electromechanical response of DE membranes is augmented to account for dynamic effects.

3.1. Geometric relationships: coordinates

In this section, a theoretical model to describe the deformation response of tubular DE transducer based on Green and Adkins' work on unreinforced elastic tubes is briefly derived. The tubular DE transducers are modeled as an elastic cylindrical membrane as shown in Fig. 2. From the symmetry of the problem and the assumption that the membrane is very thin compared with the cylinder's radius, the state of stress is considered nearly constant throughout the thickness (elastic membrane theory assumption). A set of cylindrical polar coordinates (R, Θ, η) at the midplane are employed in the undeformed state. The initial length and radius of the cylindrical membrane are given by L_0 and R, respectively. The deformations of the tubular transducer are considered to be entirely symmetric with respect to the z-axis. The meridian length of the cylindrical membrane is denoted η in the undeformed state and ξ in the deformed state. It follows that the principal directions at any point in the deformed membrane coincides with the deformed coordinates (r, θ, z), and the principal extension ratios are denoted as λ_1, λ_2, and λ_3. Specifically, λ_1 and λ_2 are the meridional and latitudinal stretch ratios that define the deformation and λ_3 is the thickness stretch ratio.

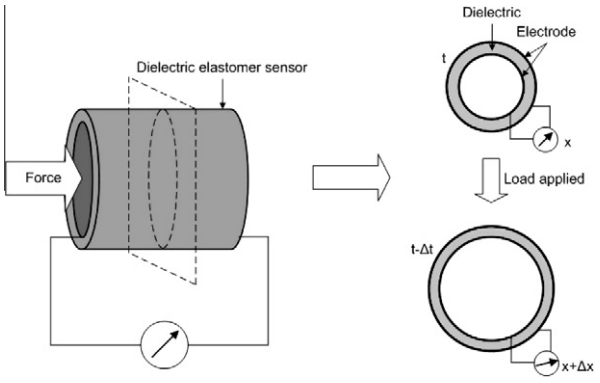

Fig. 1a. Schematic of pressure/strains sensing using a dielectric elastomer.

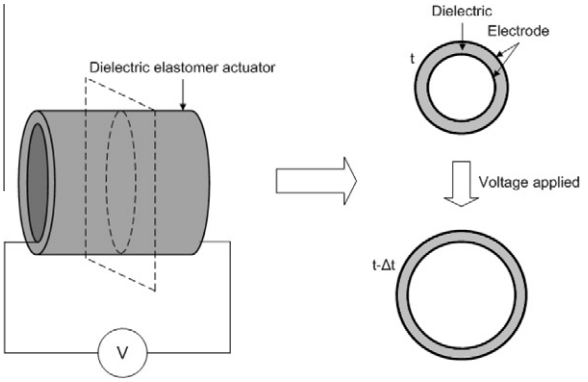

Fig. 1b. Schematic of actuation using a dielectric elastomer.

$$r = r(\xi), \quad \theta = \Theta, \quad z = z(\xi)$$
$$\lambda_1 = \frac{d\xi}{d\eta}, \quad \lambda_2 = \frac{r}{R}, \quad \lambda_3 = \frac{h}{h_0}, \tag{1}$$

where $2h_0$ and $2h$ are the undeformed and deformed thickness of the membrane.

3.2. Material modeling: electroelastic stress and strain energy function

It is assumed that the elastic dielectric material is homogenous, isotropic and electrically linear, so that there is no direct coupling between the mechanical and the electrical response. We hypothesize that the stress for the material can be written as the sum of the elastic and Maxwell stresses. Therefore, the total stresses are divided into the two parts, mechanical and electrical portion. The mechanical portion is determined by an elastic strain energy function (Mooney–Rivlin function). The electrical portion is given by the Maxwell stress. In accordance with Adkins' and Rivlin's solution approach, we presume that the applied forces normal to the cylindrical surfaces are negligible in comparison to the in-plane stresses and set $n_3 = 0$. The stress components of the membrane are then given by

$$n_1 = 2\left(\lambda_2^2 - \frac{1}{\lambda_1^2\lambda_2^2}\right)\left(\frac{\partial W}{\partial I_1} + \lambda_1^2\frac{\partial W}{\partial I_2}\right) - \frac{1}{2}\left(\varepsilon_0\varepsilon_r\left(\frac{V}{h\lambda_3}\right)^2\right),$$
$$n_2 = 2\left(\lambda_1^2 - \frac{1}{\lambda_1^2\lambda_2^2}\right)\left(\frac{\partial W}{\partial I_1} + \lambda_2^2\frac{\partial W}{\partial I_2}\right) - \frac{1}{2}\left(\varepsilon_0\varepsilon_r\left(\frac{V}{h\lambda_3}\right)^2\right), \tag{2}$$
$$n_3 = 0,$$

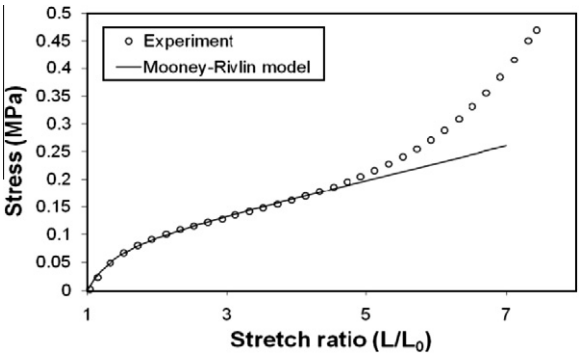

Fig. 3. Stress vs stretch data for VHB 4905 samples compared with Mooney–Rivlin model.

where n_1, n_2, and n_3 are the meridional, radial, and thickness stress components and W is a Mooney–Rivlin energy function.

Fig. 3 shows the fit of the strain energy function with experimental uniaxial data for 3M VHB 4905. The Mooney–Rivlin model fits well with experimental data up to a stretch ratio around 4.

For simplification of the partial differential equations using the finite difference scheme, the Mooney–Rivlin function is employed for describing the stress–strain behavior of dielectric elastomers (VHB 4905 & Silicone). The Mooney–Rivlin function has the form,

$$W = C_1(I_1 - 3) + C_2(I_2 - 3), \tag{3}$$

where I_1 and I_2 are strain invariants and C_i (i = 1 and 2) are Mooney–Rivlin constants determined from uniaxial extension tests on rectangular samples supporting a uniformly distributed axial load (Table 1) (Son and Goulbourne, 2009).

During deformation, the initial thickness $2h_0$ of the membrane becomes $2\lambda_3 h_0$ and the stress resultants are obtained by integrating over the deformed thickness

Table 1
Mooney–Rivlin constants for VHB 4905 and silicone.

Mooney–Rivlin constants	C_1 (kPa)	C_2 (kPa)
VHB 4905	16	7.3
Silicone	163	34.2

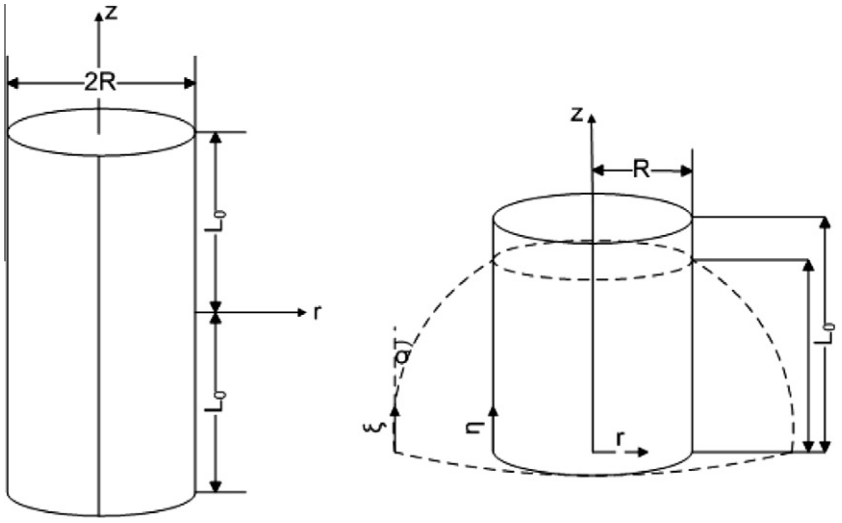

Fig. 2. An undeformed cylindrical membrane (left). Half of the undeformed and deformed membrane (right).

$$N_1 = 2\lambda_3 h_0 n_1 = 2\lambda_3 h_0 \left\{ 2\left(\lambda_2^2 - \frac{1}{\lambda_1^2\lambda_2^2}\right)\left(\frac{\partial W}{\partial I_1} + \lambda_1^2 \frac{\partial W}{\partial I_2}\right) - \frac{1}{2}\left(\varepsilon_0\varepsilon_r\left(\frac{V}{h\lambda_3}\right)^2\right)\right\},$$
$$N_2 = 2\lambda_3 h_0 n_2 = 2\lambda_3 h_0 \left\{ 2\left(\lambda_1^2 - \frac{1}{\lambda_1^2\lambda_2^2}\right)\left(\frac{\partial W}{\partial I_1} + \lambda_2^2 \frac{\partial W}{\partial I_2}\right) - \frac{1}{2}\left(\varepsilon_0\varepsilon_r\left(\frac{V}{h\lambda_3}\right)^2\right)\right\}. \quad (4)$$

3.3. Equations of motion for tubular DE membranes

The equations of motion in the meridional and radial directions are expressed as,

$$\frac{dN_1}{d\xi} + \frac{N_1}{r}\frac{dr}{d\xi} - \frac{N_2}{r}\frac{dr}{d\xi} = 2h_0\rho R\frac{d^2\xi}{dt^2},$$
$$P - \kappa_1 N_1 - \kappa_2 N_2 = 2h_0\rho R\frac{d^2 r}{dt^2}, \quad (5)$$

where κ_1 and κ_2 are the principal curvatures given by,

$$\kappa_1 = \frac{-d^2r/d\xi^2}{(1-(d^2r/d\xi^2)^2)^{1/2}} \quad \text{and} \quad \kappa_2 = \frac{1}{r}(1-(dr/d\xi)^2)^{1/2}. \quad (6)$$

For simplification, it is assumed that inertia effects in the meridional direction are negligible. Therefore, the first equation of motion in Eq. (5) becomes an equilibrium equation due to $d^2\xi/dt^2 = 0$ and results in only the second equation of motion in Eq. (6) to solve.

The independent variable ξ in the deformed state is rewritten as the independent variable η in the undeformed state by using the chain rule.

$$\frac{dr}{d\xi} = \frac{R}{\lambda_1}\frac{d\lambda_2}{d\eta},$$
$$\frac{d^2r}{d\xi^2} = \frac{d}{d\xi}\left(\frac{R}{\lambda_1}\frac{d\lambda_2}{d\eta}\right) = \frac{1}{\lambda_1}\frac{d}{d\eta}\left(\frac{R}{\lambda_1}\frac{d\lambda_2}{d\eta}\right). \quad (7)$$

Therefore, Eqs. (5) and (6) can be rewritten using Eq. (7)

$$\frac{dN_1}{d\xi} + \frac{N_1}{r}\frac{dr}{d\xi} - \frac{N_2}{r}\frac{dr}{d\xi} = 0,$$
$$P - \kappa_1 N_1 - \kappa_2 N_2 = 2h_0\rho R\frac{d^2\lambda_2}{dt^2}, \quad (8)$$

$$\kappa_1 = -\frac{\left(\frac{1}{\lambda_1}\frac{d}{d\eta}\left(\frac{R}{\lambda_1}\frac{d\lambda_2}{d\eta}\right)\right)^2}{\sqrt{\left(1-(Rd\lambda_2/\lambda_1 d\eta)^2\right)}}, \quad \kappa_2 = \sqrt{\frac{1}{\lambda_2}\left(\frac{1}{R^2} - \left(\frac{1}{\lambda_1}\frac{d\lambda_2}{d\eta}\right)^2\right)}. \quad (9)$$

For dynamic solutions, the initial conditions are the radial deformation and deformation rate which are defined at $t = 0$. Boundary conditions are defined at one end and the midlength of the cylinder. At the fixed end, the radial deformation is equal to zero and the curvature in the meridional direction at the middle of the membrane is zero.

$$\lambda_2(\eta, 0) = \lambda_2(\eta), \quad \frac{d\lambda_2}{dt}(\eta, 0) = 0, \quad (10)$$

$$\lambda_2(L_0, t) = 1, \quad \kappa_1 = -\left.\frac{\left(\frac{1}{\lambda_1}\frac{d}{d\eta}\left(\frac{R}{\lambda_1}\frac{d\lambda_2}{d\eta}\right)\right)^2}{(1-(Rd\lambda_2/\lambda_1 d\eta)^2)^{1/2}}\right|_{\eta=0} = 0. \quad (11)$$

The capacitance of the deformed tubular sensor is modeled by utilizing large deformation membrane theory and electrostatics. The approach is based on the assumption that the membrane is very thin compared with the tubular sensor's radius, as well as axisymmetric deformation (Goulbourne and Son, 2008). The capacitance of the unit volume of the deformed tubular membrane is calculated using electrostatics. The total capacitance of the tubular membrane is obtained by integrating the capacitance of the unit volume with respect to the axis. The capacitance for an axisymmetric tubular membrane is

$$C = \varepsilon_0\varepsilon_r 2\pi R\int_1^{\lambda_2(0)} \frac{1}{\ln\left(\frac{R\lambda_2 + h_0\frac{1}{\lambda_1\lambda_2}}{R\lambda_2 - h_0\frac{1}{\lambda_1\lambda_2}}\right)}\frac{1}{\tan\sigma}d\lambda_2, \quad (12)$$

where σ is the angle between membrane curve and vertical direction in Fig. 1, ε_r is the relative permittivity and ε_0 is the vacuum permittivity.

3.4. Numerical solution procedure

In order to obtain the numerical solutions for the dynamic response of tubular DE transducers, a finite different scheme (forward difference method) is employed. The equation of motion, Eq. (8) is second order in time and space and thus impossible to solve analytically. The first and second derivatives with respect to time and space are

$$\lambda_1 = \lambda_{1,i}^j, \quad \lambda_2 = \lambda_{2,i}^j,$$
$$\frac{d\lambda_1}{d\eta} = \frac{\lambda_{1,i+1}^j - \lambda_{1,i}^j}{h}, \quad \frac{d\lambda_2}{d\eta} = \frac{\lambda_{2,i+1}^j - \lambda_{2,i}^j}{h},$$
$$\frac{d^2\lambda_2}{d\eta^2} = \frac{\lambda_{2,i+2}^j - 2\lambda_{2,i+1}^j + \lambda_{2,i}^j}{h^2},$$
$$\frac{d^2\lambda_2}{dt^2} = \frac{\lambda_{2,i}^{j+2} - 2\lambda_{2,i}^{j+1} + \lambda_{2,i}^j}{k^2}, \quad (13)$$

where i and j are the space and time indices, respectively as well as h and k are space and time increments.

The parameters h and k are defined as

$$h = \frac{L_0}{n}, \quad k = \frac{T}{m}, \quad (14)$$

where n and m are the space and time component number and T is the time period.

The equation of motion, initial conditions, and boundary conditions are rewritten by using the finite different method as

$$P - \kappa_1 N_1 - \kappa_2 N_2 = 2h_0\rho R\frac{\lambda_{2,i}^{j+2} - 2\lambda_{2,i}^{j+1} + \lambda_{2,i}^j}{k^2}, \quad (15)$$

$$\lambda_2(\eta, 0) = \lambda_{2,i}^0, \quad \frac{d\lambda_2}{dt}(\eta, 0) = \frac{\lambda_{2,i}^1 - \lambda_{2,i}^0}{k} = 0, \quad (16)$$

$$\lambda_{2,n}^j = 1, \quad \kappa_1 = -\left.\frac{\left(\frac{1}{\lambda_{1,0}^j}\frac{d}{d\eta}\left(\frac{R}{\lambda_{1,0}^j}\frac{\lambda_{2,1}^j - \lambda_{2,0}^j}{h}\right)\right)^2}{\left(1-\left(\frac{R}{\lambda_{1,0}^j}\frac{\lambda_{2,1}^j - \lambda_{2,0}^j}{h}\right)^2\right)^{1/2}}\right|_{\eta=0} = 0. \quad (17)$$

In the case of $j = 0$, Eq. (15) by inserting Eq. (16) becomes

$$\lambda_{2,i}^2 = \frac{k^2}{2h_0\rho R}(P - \kappa_1 N_1 - \kappa_2 N_2) + \lambda_{2,i}^1. \quad (18)$$

To ensure convergence of the solution, the k value is changed until $\lambda_{2,n}^2$ converges to 1, which matches with boundary condition, Eq. (16). Considering $j = 1$, Eq. (15) becomes

$$\lambda_{2,i}^3 = \frac{k^2}{2h_0\rho R}(P - \kappa_1 N_1 - \kappa_2 N_2) + 2\lambda_{2,i}^2 - \lambda_{2,i}^1. \quad (19)$$

Similarly, the solution at j = 1 is obtained when $\lambda_{2,n}^2$ is converged to 1 by changing the k value. By repeating the previous steps for $j = 2,3,4,\ldots,m$, numerical solutions are obtained.

Table 2
The initial dimensions of tubular DE sensor and actuator (VHB 4905 and silicone film).

Sample	R (mm)	L (mm)	t (mm)
VHB sensor	9.56	20	0.5
Silicone sensor	9.56	20	0.1
Silicone actuator	9.56	20	0.2

4. Experimental and numerical results

In this section, the dynamic characteristics of tubular VHB and silicone transducers are presented. In Section 4.1, the experimental setup for the dynamic response is described. In Section 4.2, the sensing response is analyzed. Specifically, the frequency response is monitored while dynamic pressure is applied at various frequencies. In Section 4.3, the actuation response is described. The response is measured while dynamic high voltage is applied with various frequencies. For the validation of our modeling approach, the experimental results are compared with the numerical results, which are simulated using finite difference scheme, described in Section 3.4.

4.1. Experimental setup

In this section, the sample preparation procedure and experimental setup are presented. Polyacrylate and silicone films are used to make tubular DE samples. 3M VHB is commercially available and silicone films are fabricated using a spincoater (Son and Goulbourne, 2009) and the initial dimensions are given in Table 2. For a length to radius ratio of one, the edge constraints could limit the radial deformation of the middle cross-section of the sample. Fig. 4 shows the effect of the length–radius ratio (L/R) on the radial deformation. According to Fig. 4, the effect of L/R is negligible within pressure range considered in this research (0–2000 Pa).

In the experimental setup (Fig. 5), dynamic responses of tubular DE sensor/actuator are obtained by measuring the capacitance and the radial deformation at the midpoint of the transducer, which are measured by a capacitance meter (Model 3000, GLK) and a triangular optical laser sensor (Model LTC-050-20, MTI INSTRUMENT, INC). Dynamic pressure is used to inflate the tubular sensor and actuator by a combination of a syringe (140CC), linear stage (NLS4 Series linear stage, Newmark systems, INC) and solenoid valves (SY3340-SGZ, SMC), and measured by a pressure sensor (163PC01D36, OMEGA). A high voltage dynamic signal is applied by supplying a LabVIEW generated signal to an amplifier (Model 610E, Trek, INC).

For the tubular DE sensor experiment, the fabricated tubular samples are attached to a frame (Fig. 5) and a dynamic pressure (1400 and 2000 Pa) is applied with excitation frequencies ranging from 0 to 5.0 Hz. Higher frequencies (2.5–5.0 Hz) are generated by opening and closing the solenoid valves. For even higher frequencies, modifications to the experimental setup would be needed. A schematic of the experimental setup is given in Fig. 3. For the tubular DE actuator experiment, the linear stage and syringe provide a static pressure (2000 Pa) and a dynamic voltage (4.5 kV) is applied with excitation frequencies ranging from 0 to 30 Hz. In each of these experiments, 3 tests for 4 each samples are performed.

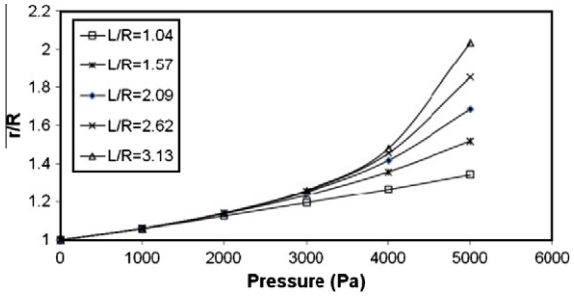

Fig. 4. The effect of L/R on the radial deformation of the sample.

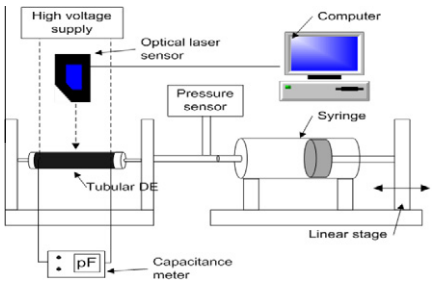

Fig. 5. Experimental setup for dynamic response of tubular DE sensors and actuators.

4.2. Dynamic response of tubular DE sensors with dynamic pressure input

The initial capacitance value of the VHB sensor is 85 pF and the initial dimensions of the sensor are given in Table 2. Figs. 6a and 6b show the capacitance change and deformed radius of the tubular VHB sensor while a dynamic pressure (2000 Pa) is applied at 0.3 Hz. At a low frequency (0.3 Hz), there is no delay between the pressure signal, the measured capacitance, and deformed radius. The maximum values of the measured capacitance and deformed radius are consistently measured to be 107 pF and 11 mm as shown in Figs. 6a and 6b. That is to say, the VHB sensor

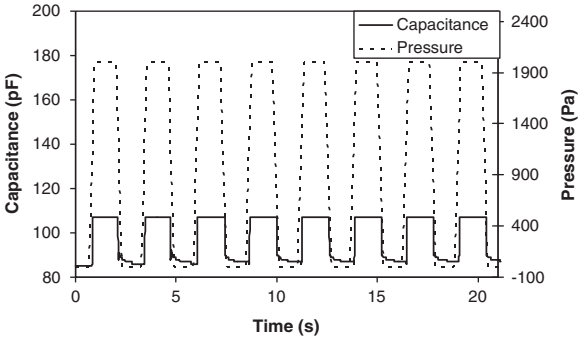

Fig. 6a. Dynamic capacitance of a VHB sensor at 0.3 Hz.

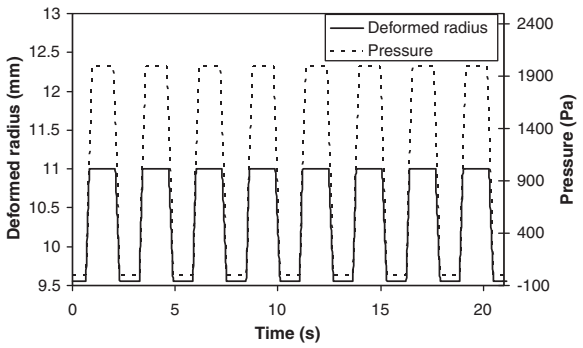

Fig. 6b. Radial deformation of a tubular VHB sensor at 0.3 Hz.

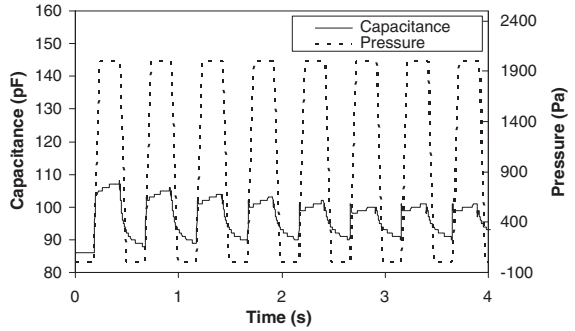

Fig. 7a. Dynamic capacitance of a VHB sensor at 2.0 Hz.

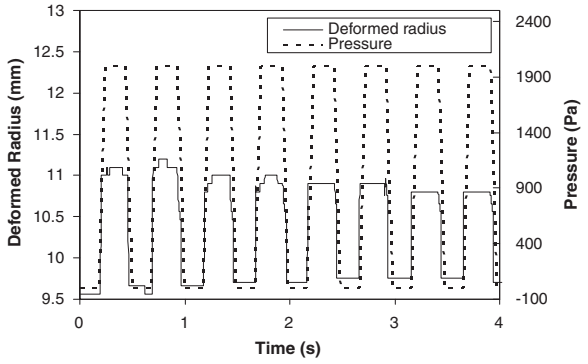

Fig. 7b. Radial deformation of a tubular VHB sensor at 2.0 Hz.

has a good quasi-static sensing response. Figs. 7a and 7b show the sensing response of the VHB sensor at 2.0 Hz. For a 2.0 Hz signal of amplitude 2000 Pa, the capacitance signal is not identical to the dynamic pressure signal and the maximum value of capacitance decays with time. To understand the output signal further, which exhibits a definite rise and decay time, a comparison between the radial deformation and the input pressure is conducted. Fig. 7b shows that the mechanical response (radial deformation) of the VHB sensor at 2.0 Hz is identical to the pressure signal and there is no delay. Therefore, the dissimilarity between the capacitance and the pressure signal is electrical in nature. There is an apparent time required for charging/discharging the VHB sensor. That is to say, the VHB tubular sensor is capacitive in nature. Additionally, the amplitude of the radial deformation decreases as the cycle is repeated. This is due to the material viscoelasticity. VHB sensors do not have a linear dynamic response at frequencies above 2.0 Hz. The sensor has good quasi-static behavior, but a poor dynamic response above 2.0 Hz.

Between the frequency range of 0–5.0 Hz, the capacitance change and radial deformation of the tubular silicone sensor are monitored while a dynamic pressure is applied. Initially, the capacitance value of the depressurized sensor is 435 pF. Initial dimensions of the sensor are given in Table 2. It should be noted that the dynamic pressure profile is not a perfect rectangular shape. It is expected that the dynamic response of the silicone sensor shows linearity in proportion to the dynamic pressure. In Fig. 8, the somewhat quasi-static response of a silicone sensor (0.17 Hz) is shown. In detail, Fig. 8a shows that the measured capacitance is identical to the dynamic pressure signal and the dynamic maximum value of the capacitance is 485 pF. That is to say, the silicone sensor shows a linear relationship between the mechanical input and the electrical output. Comparatively, Fig. 8b shows the deformation of the membrane corresponding to the measured capacitance in Fig. 8a. Fig. 9 illustrates the dynamic response of the silicone sensor

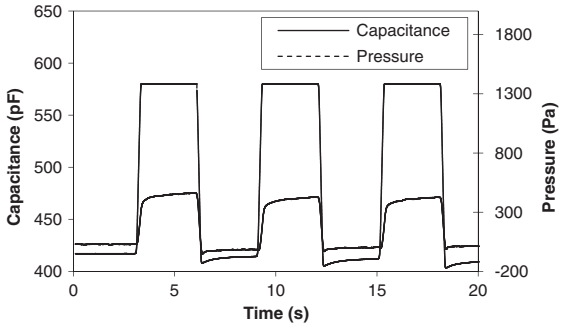

Fig. 8a. Capacitance change of a tubular silicone sensor at 0.17 Hz.

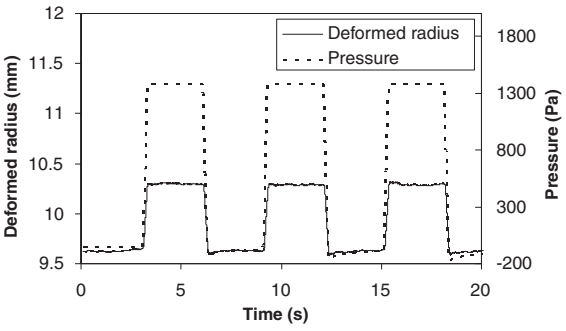

Fig. 8b. Radial deformation of a tubular silicone sensor at 0.17 Hz.

at 4.7 Hz. In Fig. 9a, it is shown that the maximum value of the capacitance is 485 pF, but there is a slight delay between the mechanical input and the electrical output. Similarly in Fig. 9b, the maximum radial deformation is 10.30 mm at a pressure of 1400 Pa but, there is almost no delay or time lag between the mechanical input and the output. Therefore, the delay in Fig. 9a exists only between the mechanical input and the electrical output. This appears to be related to the electrical charging and discharging time for the silicone sensor.

In summary, both VHB and silicone sensors show good quasi-static sensing behavior. The experimental analysis indicates that the maximum capacitance value of the VHB sensor at 2.0 Hz decays in time and the electrical output signal is delayed due to charging/discharging time (around 0.3 s at 2.0 Hz), so that the VHB sensor shows poor dynamic response. On the other hand, the silicone sensor outputs a non-decaying signal and the charging/discharging time is significantly less around 0.05 s at 4.7 Hz. Therefore, it can be concluded that the silicone sensor has a wider dynamic range in comparison to VHB sensors.

Figs. 10a and 10b show a comparison between numerical and experimental results for the silicone sensor at 1400 Pa at 5.0 Hz.

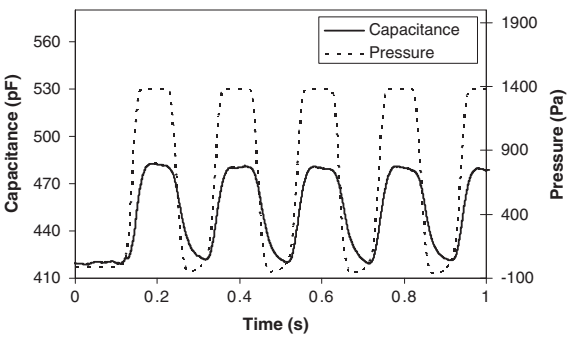

Fig. 9a. Capacitance change of a tubular silicone sensor at 4.7 Hz.

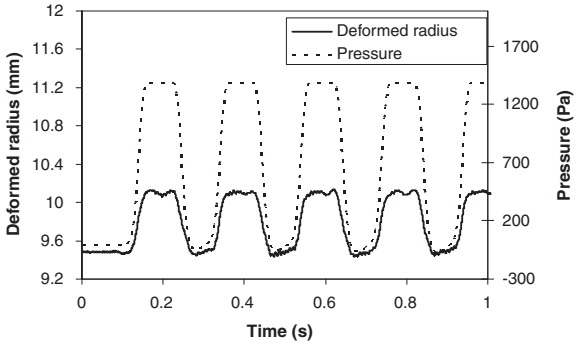

Fig. 9b. Radial deformation of a tubular silicone sensor at 4.7 Hz.

In Figs. 10a and 10b, there are differences between the numerical (rectangular) and experimental results (close to trapezoid), although the minimum and maximum values have a good correlation. The trapezoidal curve of the experimental capacitance results in Fig. 10a is due to the discharging and charging time for the silicone sensor as well as the trapezoidal shape of the dynamic pressure input in Fig. 8. Also, the measured radial deformation in Fig. 10b comes from the trapezoidal shape of the experimental pressure input. Since these factors in the experiment are not included in the theoretical model, the differences in the results are expected. The comparison between maximum/minimum values of numerical and experimental capacitance and radial deformation in Fig. 10 shows within 3% overall error.

4.3. Dynamic response of tubular DE actuators with dynamic voltage input

A series of experiments were conducted in which a dynamic voltage input between 0 and 30 Hz with an amplitude of 4.5 kV

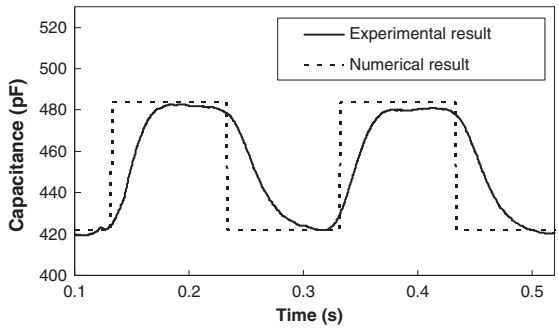

Fig. 10a. Comparison of numerical and experimental results for capacitance sensing (5.0 Hz).

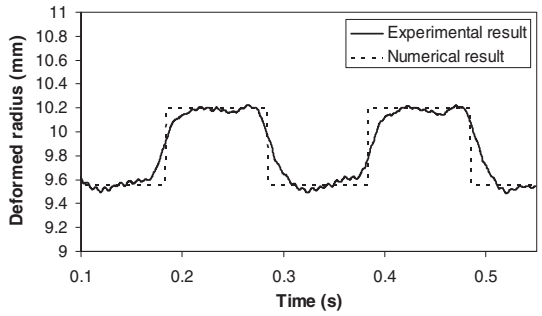

Fig. 10b. Comparison of radial deformation between numerical and experimental results (5.0 Hz).

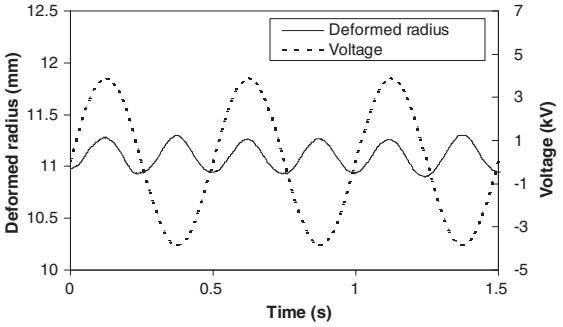

Fig. 11. Radial deformation of tubular silicone actuator at 2.0 Hz.

was applied to the tubular membrane. The initial dimensions of the transducers are given in Table 2. Radial deformation of the initially pressurized tubular silicone actuator (2000 Pa) is measured while a dynamic voltage is applied. The radius of the tubular silicone actuator with the static pressure is 10.80 mm. Figs. 11 and 12 describe the relationship between the electrical input (voltage) and the mechanical output (radial deformation) for the given frequency values. Since there is a linear relationship and no delay between electrical input and mechanical output, good dynamic actuation responses of the tubular silicone actuator are shown. The normalized maximum amplitudes ((Deformed radius-10.80)/(10.80–9.56)) for 3 sets of voltage sweeps (1–30 Hz) are shown in Fig. 13. The maximum amplitude averages around 0.5 below 15 Hz, and reaches 0.6 at 20–22 Hz and then steadily declines with increasing frequency.

Figs. 14 and 15 show the comparison between numerical and experimental results for a 4.5 kV signal at 2.0 and 10 Hz. The experimental curves in Figs. 14 and 15 accord well with the numerical results. The correlation between numerical and experimental results are within 3% overall error. Therefore, the modeling approach that is proposed in this paper is validated by these experimental results.

5. Summary

In this paper, the dynamic actuation and sensing response of tubular dielectric elastomers was discussed. A theoretical background for the dynamic model based on a large deformation theory for DE membranes and electrostatics was presented. Numerical results were obtained by employing a finite difference scheme to solve the PDEs. The experiments indicate that both VHB and silicone sensors have good quasi-static sensing behavior. However, for the dynamic response within a limited frequency range, the VHB sensor shows poor response after 2.0 Hz and 13% radial strain

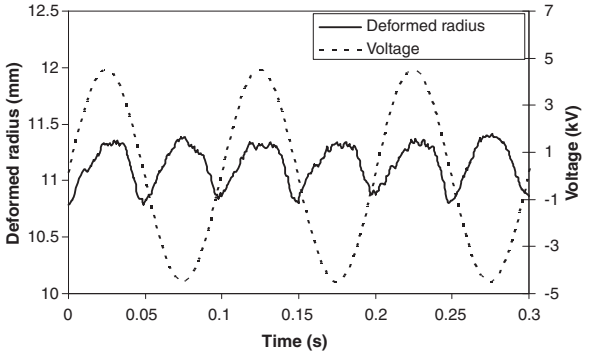

Fig. 12. Radial deformation of tubular silicone actuator at 10 Hz.

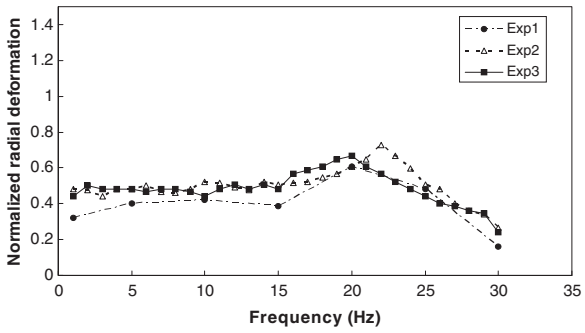

Fig. 13. Dynamic actuation peak amplitudes for voltage frequencies, 1–30 Hz.

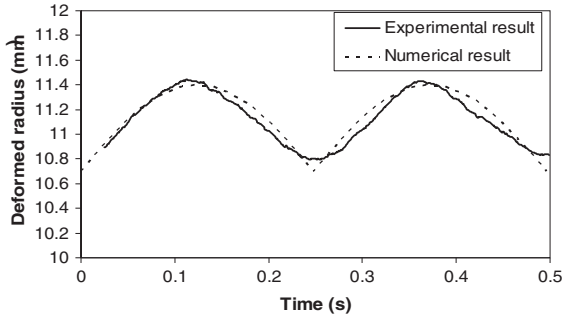

Fig. 14. Comparison between numerical and experimental results (2.0 Hz).

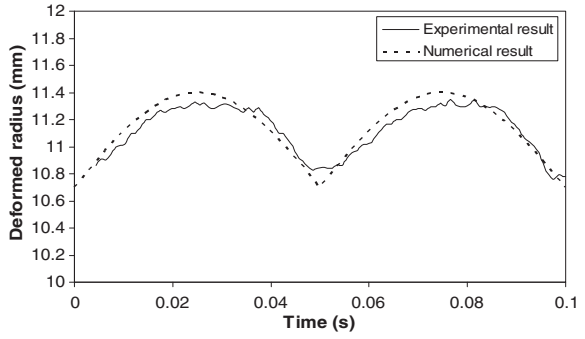

Fig. 15. Comparison between numerical and experimental result (10 Hz).

under an applied dynamic pressure. The tubular silicone sensor shows good sensing response at higher frequencies up to 5.0 Hz and 8% radial strain. Tubular silicone actuators were assembled and dynamically actuated with a voltage signal (4.5 kV) at 0–30 Hz. From the results it can be concluded that tubular silicone transducers have a better dynamic sensing and actuation response in the frequency range analyzed in this research. Comparison between the maximum values of numerical and experimental results for the silicone sensor and actuator shows good agreement with 3% overall error. This shows that the dynamic model and solution approach based on the finite difference method is a good tool for predicting the finite dynamic deformation of tubular DE sensors and actuators.

References

Adkins, J.E., Rivlin, R.S., 1952. Large elastic deformations of isotropic materials – IX. Deformation of thin shells. Philosophical Transactions 244 (888), 505–531.

Adkins, J.E., Rivlin, R.S., 1955. Large elastic deformations of isotropic materials X. Reinforced by in extensible cords. Royal Society of London – Philosophical Transactions Series A 2418, 201–223.

Carpi, F., De Rossi, D., 2004. Dielectric elastomer cylindrical actuators: electromechanical modelling and experimental evaluation. Materials Science and Engineering C 24 (4), 555–562.

Carpi, F., Migliore, A., et al., 2005. Helical dielectric elastomer actuators. Smart Materials and Structures 14 (Copyright 2005, IEE), 1210–1216.

Carpi, F., Rossi, D.D., et al., 2008. Dielectric elastomers as electromechanical transducers. Fundamentals, Materials, Devices, Models and Applications of an Emerging Electroactive Polymer Technology. Elsevier, Oxford.

Verron, E., Khayat, R.E., Derdouri, A., Peseux, B., 1999. Dynamic inflation of hyperelastic spherical membranes. Journal of Rheology 43 (5), 1083–1097.

Fox, J.W., 2007. Electromechanical characterization of the static and dynamic response of dielectric elastomer membranes. Mechanical Engineering. Virginia Polytechnic Institute and State University. Master of Science, Blackburg.

Fox, J.W., Goulbourne, N.C., 2006. A study on the effect of flexible electrodes and passive layers on the performance of dielectric elastomer membranes. In: Proceedings ASME IMECE, Chicago.

Fox, J.W., Goulbourne, N.C., 2008. On the dynamic electromechanical loading of dielectric elastomer membranes. Journal of the Mechanics and Physics of Solids 56 (8), 2669–2686.

Goulbourne, D.N.C., Son, S., et al., 2007. Self-sensing McKibben actuators using dielectric elastomer sensors, San Diego, CA, United States, SPIE, Bellingham WA, WA 98227-0010, United States.

Goulbourne, N., Mockensturm, E., et al., 2005. A nonlinear model for dielectric elastomer membranes. Journal of Applied Mechanics, Transactions ASME 72 (6), 899–906.

Goulbourne, N.C., Son, S., 2008. Numerical and experimental analysis of McKibben actuators and dielectric elastomer sensors. Seattle, WA, United States American Society of Mechanical Engineers, New York, NY 10016-5990, United States.

Jenkins, C.H., 1996. Nonlinear dynamic response of membranes: state of the art – update. Applied Mechanics Reviews 49 (10 Pt. 2), 41–48.

Kornbluh, R., 2004. Dielectric elastomer artificial muscle for actuation, sensing, generation, and intelligent structures. Materials Technology 19 (4), 216–224.

Kydoniefs, A.D., 1968. Finite axisymmetric deformations of an initially cylindrical elastic membrane enclosing a rigid body. Quarterly Journal of Mechanics and Applied Mathematics 22, 319–331.

Kydoniefs, A.D., 1969. Finite axisymmetric deformations of an initially cylindrical membrane reinforced with inextensible cords. Quarterly Journal of Mechanics and Applied Mathematics 23, 481–488.

Kydoniefs, A.D., 1972. Finite axisymmetric deformations of initially cylindrical reinforced membranes. Rubber Chemistry and Technology 45 (6), 1677–1683.

Matsikoudi-Iliopoulou, M., 1987. Finite axisymmetric deformations with torsion of an initially cylindrical membrane reinforced with one family inextensible cords. International Journal of Engineering Science 25 (6), 673–680.

Pei, Q., Rosenthal, M., et al., 2003. Multifunctional Electroelastomer Eoll Aactuators and Their Application for Biomimetic Walking Robots. The International Society for Optical Engineering, San Diego, CA, United States.

Pei, Q., Rosenthal, M., et al., 2004. Multiple-degrees-of-freedom electroelastomer roll actuators. Smart Materials and Structures 13 (5), 86–92.

Pelrine, R., Kornbluh, R., et al., 2000a. High-strain actuator materials based on dielectric elastomers. Advanced Materials 12 (16), 1223–1225.

Pelrine, R., Kornbluh, R., et al., 2000b. High-speed electrically actuated elastomers with strain greater than 100%. Science 287 (5454), 836–839.

Rosenthal, M., Bonwit, N., et al., 2007. Applications of dielectric elastomer EPAM sensors. San Diego, CA, United States, SPIE, Bellingham WA, WA 98227-0010, United States.

Sommer-Larsen, P., Hooker, J., et al., 2001. Response of dielectric elastomer actuators. Society of Photo-Optical Instrumentation Engineers, Newport Beach, CA.

Son, S., Goulbourne, N.C., 2009. Finite deformations of tubular dielectric elastomer sensors. Journal of Intelligent Material Systems and Structures 20, 2187–2199.

Tüzel, V.H., Erbay, H.A., 2004. The dynamic response of an incompressible non-linearly elastic membrane tube subjected to a dynamic extension. International Journal of Non-Linear Mechanics 39 (4), 515–537.

Verron, E., Marckmann, G., et al., 2001. Dynamic inflation of nonlinear elastic and viscoelastic rubber-like membranes. International Journal for Numerical Methods in Engineering 50 (5), 1233–1251.

Waki, M., Chiba, S., et al., 2008. Electric power from artificial muscles. OCEANS 2008 MTS/IEEE Kobe Techno-Ocean, 8-11 April 2008, Piscataway, NJ, USA, IEEE.

Yang, G., Yao, G., et al., 2005. The Strain Response of Silicone Dielectric Elastomer Actuators. International Conference on Smart Materials Structures and Systems, Bangalore.